

# Processing of mullite–glass ceramics using simplex-centroid design: Densification process dominated by liquid-phase sintering

Hugo P. A. Alves<sup>a,\*,1</sup>, Allan J. M. Araújo<sup>a,\*,1</sup>, Rivaildo M. Andrade<sup>b</sup>, Rubens A. Junior<sup>c</sup>, Heber S. Ferreira<sup>b</sup>, Wilson Acchar<sup>a</sup>, Lizandra F. A. Campos<sup>b</sup>, Daniel A. Macedo<sup>b,\*</sup>

<sup>a</sup> Materials Science and Engineering Postgraduate Program – PPGCEM, Federal University of Rio Grande do Norte – UFRN, 59078-970 Natal, Brazil

<sup>b</sup> Materials Science and Engineering Postgraduate Program, Federal University of Paraíba, 58051-900 João Pessoa, Brazil<sup>2</sup>

<sup>c</sup> Materials Science and Engineering Postgraduate Program, Federal University of Campina Grande, 58429-900 João Pessoa, Brazil

## ARTICLE INFO

### Article history:

Received 5 June 2020

Accepted 3 September 2020

Available online 5 October 2020

### Keywords:

Kaolinitic clay

Kaolin waste

Mullite

SiO<sub>2</sub>–Al<sub>2</sub>O<sub>3</sub>–K<sub>2</sub>O

Design of experiments

## ABSTRACT

Mullite is one of the preferred aluminosilicates for both traditional and advanced ceramics. This paper reports the use of simplex-centroid mixture design to prepare mullite–glass ceramics by reactive sintering. The phase composition and technological properties of formulations containing kaolinitic clay, kaolin waste and alumina were investigated after sintering at 1400 °C. The sintering behavior was assessed by dilatometry. Microstructural analysis indicated the crystalline phases mullite, residual quartz, cristobalite, and α-alumina. A glassy phase was also identified as a matrix embedding mullite grains (as seen by X-ray diffractometry and scanning electron microscopy). In kaolin waste-rich formulations, a liquid phase sintering mechanism favored the densification process and the mechanical resistance. Highly significant statistical models allow correlating the concentrations of raw materials with linear firing shrinkage, water absorption and apparent porosity. Overall results stand out for the potential of using kaolin waste in the preparation of mullite–glass ceramics.

© 2020 SECV. Published by Elsevier España, S.L.U. This is an open access article under the CC BY-NC-ND license (<http://creativecommons.org/licenses/by-nc-nd/4.0/>).

## Procesamiento de materiales cerámicos de mullita-vidrio a través del diseño de mezclas simplex con centroide: proceso de densificación dominado por la sinterización en fase líquida

## RESUMEN

La mullita es uno de los aluminosilicatos preferidos para la producción de cerámicas tradicionales como avanzadas. Este artículo informa sobre el uso del diseño de mezclas simplex con centroide para preparar materiales cerámicos de mullita-vidrio a través de la

### Palabras clave:

Arcilla caolinítica

Residuo de caolín

\* Corresponding authors.

E-mail addresses: [eng.hugoplinio@gmail.com](mailto:eng.hugoplinio@gmail.com) (H.P.A. Alves), [allanmenezes@ufrn.edu.br](mailto:allanmenezes@ufrn.edu.br) (A.J.M. Araújo), [daniel.macedo@academico.ufpb.br](mailto:daniel.macedo@academico.ufpb.br) (D.A. Macedo).

<sup>1</sup> These authors contributed equally to this work.

<sup>2</sup> Address where the work was done.

<https://doi.org/10.1016/j.bsecv.2020.09.002>

0366-3175/© 2020 SECV. Published by Elsevier España, S.L.U. This is an open access article under the CC BY-NC-ND license (<http://creativecommons.org/licenses/by-nc-nd/4.0/>).

Mullita  
SiO<sub>2</sub>–Al<sub>2</sub>O<sub>3</sub>–K<sub>2</sub>O  
Diseño de experimentos

sinterización reactiva. Las fases presentes en el material y las propiedades de las formulaciones que contienen arcilla caolinítica, residuos de caolín y alúmina se investigaron después de la sinterización a 1.400 °C. El comportamiento del material cerámico sinterizado se evaluó por dilatometría. Por otra parte, el análisis microestructural mostró la presencia de fases cristalinas de mullita, cuarzo residual, cristobalita y  $\alpha$ -alúmina. También se identificó una fase vítrea como una matriz que incorpora granos de mullita (se demostró por difracción de rayos X y microscopía electrónica de barrido). En las formulaciones ricas en residuo de caolín, la sinterización en fase líquida favoreció el proceso de densificación y la resistencia mecánica. Los modelos estadísticos altamente significativos permiten relacionar las concentraciones de materias primas con la contracción de cocción lineal, la absorción de agua y la porosidad aparente. Los resultados generales destacan el uso de residuo de caolín en la preparación de materiales cerámicos tipo mullita-vidrio.

© 2020 SECV. Publicado por Elsevier España, S.L.U. Este es un artículo Open Access bajo la licencia CC BY-NC-ND (<http://creativecommons.org/licenses/by-nc-nd/4.0/>).

## Introduction

Mullite is one of the most essential aluminosilicates, being the only stable intermediate compound in the SiO<sub>2</sub>–Al<sub>2</sub>O<sub>3</sub> system, with the composition 3Al<sub>2</sub>O<sub>3</sub>·2SiO<sub>2</sub> corresponding to 71.8 wt.% Al<sub>2</sub>O<sub>3</sub> [1]. The technological importance, combined with the rare occurrence in nature, highlights the necessity of research on mullite synthesis [2]. Several routes, such as sol–gel process [3], hydrothermal processes [4], chemical vapor deposition [5], and reactive sintering [6] have been used for the synthesis of this mineral. On the other hand, expensive chemical precursors are commonly used. Therefore, it is necessary to use economically viable precursors as a way of reducing production costs, highlighting the potential of kaolin waste for this application [7,8].

The kaolin waste comes from the kaolin mining and processing industry, in which it produces thousands of tons of kaolin per year, being an important economical segment [9]. The recycling and reuse of waste must be seen not only as economic feasibility but also from an environmental point of view. With this in mind, the need to provide a higher added value to the obtained products gains evidence and importance, encouraging the absorption of waste in the productive environment and favoring the culture of reuse [10,11]. As discussed above, the stoichiometric mullite has a molar ratio of 3:2 for alumina:silica; however, kaolin waste and kaolin clay have been reported with higher SiO<sub>2</sub> content than Al<sub>2</sub>O<sub>3</sub> [12]. In this regard, highly reactive alumina has been used with these raw materials to achieve 3Al<sub>2</sub>O<sub>3</sub>·2SiO<sub>2</sub> [13]. The mixture of raw materials is of fundamental importance for several technological sectors, and the properties of the final product can be optimized through the appropriate formulation of raw materials [14]. In this sense, the use of designed experiments has found broad application, both in laboratory research and in industrial developments [15,16]. In a previous work [13], 2<sup>2</sup> factorial designs were used to study the factors applied pressing pressure and firing temperature for the optimization of solid-state synthesis and characterization of alumina-based composites from kaolin clay + aluminum hydroxide and kaolin waste + aluminum hydroxide; nonetheless, the levels of one factor are independent of the levels of another factor. In mixture experiments, the factors are components of

a mixture and, as a consequence, their levels are not independent [17]. With this in mind, the simplex-centroid mixture design was used in this work to prepare ceramic formulations containing kaolin clay, kaolin waste and alumina. In this regard, a triaxial diagram was adopted using such raw materials and the analysis of variance (ANOVA) and response surface methodology were applied to evaluate the physical properties. A comprehensive compositional, microstructural, and technological analysis was carried out. Our results stand out for the potential of using kaolin waste in the development of high value-added products, such as mullite–glass ceramics.

## Materials and methods

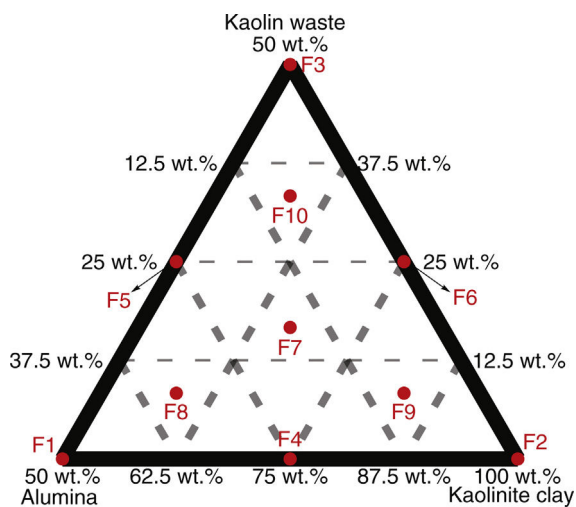
Ceramic formulations were prepared based on the simplex-centroid mixture design using kaolin clay, kaolin waste (both from the state of Paraíba – Brazil) and alumina as starting materials. The alumina powder was obtained from the calcination of aluminum hydroxide at 1000 °C, as reported in previous works [18,19]. Restrictions related to the amount of each raw material were used as provided in Table S1. Kaolin is a good candidate to prepare mullite-based ceramics by conventional sintering [20,21]. Our group has reported the increase in the amount of glassy phase with increasing the kaolin waste content in mixtures with clay [8,22]. In order to obtain mullite–glass composites, kaolin clay content ranged from 50 to 100 wt.% in formulations with kaolin waste and extra alumina to react with SiO<sub>2</sub>. The used formulations are shown in Table 1. Four replicates were run for each formulation. The design points obtained according to a {3,2} simplex-centroid design augmented with interior points are schematized in Fig. 1.

Starting materials comprising a kaolin clay, kaolin waste and alumina were ball milled in aqueous medium for 5 h using a weight ratio of powder to alumina balls of 1:3. Suspensions were dried at 110 °C for 24 h and the resulting powders were deagglomerated and sieved. Rectangular ceramic bodies (61 × 21 × 7.6 mm, using 6.5 wt.% of water as a binding agent) were shaped by uniaxial pressing at 40 MPa and subsequently fired at 1400 °C for 3 h in air using a heating rate of 3 °C/min.

The chemical composition of starting powders was obtained by X-ray fluorescence spectroscopy (EDX – Shimadzu,

**Table 1 – Ceramic formulations using an augmented simplex-centroid design.**

Formulation	Raw material proportion/design point (wt.%)		
	Kaolinitic clay	Kaolin waste	Alumina
F1	50.00	0.00	50.00
F2	100.00	0.00	0.00
F3	50.00	50.00	0.00
F4	75.00	0.00	25.00
F5	50.00	25.00	25.00
F6	75.00	25.00	0.00
F7	66.67	16.67	16.67
F8	58.33	8.33	33.33
F9	83.33	8.33	8.33
F10	58.33	33.33	8.33

**Fig. 1 – Simplex-centroid design used to prepare the ceramic formulations.**

EDX-700). Mineralogical characterization of the raw materials (reported in a previous work [12]) and sintered samples was performed by powder X-ray diffractometry. (XRD – Shimadzu, XRD 7000, using Cu-K $\alpha$  radiation, 30 mA and 40 kV). The crystalline phases were identified by comparing the experimental data with patterns registered in the ICDD (International Center for Diffraction Data). Microstructural analysis of fracture samples (without any surface treatment) was carried out using scanning electron microscopy (Supra 35-VP Model, Carl Zeiss and Quanta 450, FEI). Sintering shrinkage behaviors of green rectangular samples were measured by dilatometry using a horizontal pushrod Netzsch DIL 402 PC dilatometer in air from 30 to 1500 °C with an Al<sub>2</sub>O<sub>3</sub> Netzsch standard as reference.

The apparent porosity (AP), density (AD) and water absorption (WA) of sintered samples (rectangular bodies) were determined following the Archimedes' principle in distilled water. Linear firing shrinkage ( $\Delta L$ ) was determined by geometric measurements before and after the sintering process. The mechanical properties of sintered samples were investigated by using the three-point bending test following the ASTM C674 [23]. The physical-mechanical properties were acquired using

the relations described Eqs. (1)–(5) [24].

$$AP (\%) = \frac{W(\text{water-saturated}) - W(\text{sintered})}{W(\text{water-saturated}) - W(\text{water-immersed})} \times 100 \quad (1)$$

$$AD (\text{g/cm}^3) = \frac{w(\text{sintered})}{W(\text{water-saturated}) - W(\text{water-immersed})} \times \rho \quad (2)$$

$$WA (\%) = \frac{W(\text{water-saturated}) - w(\text{sintered})}{W(\text{saturated})} \times 100 \quad (3)$$

$$\Delta L (\%) = \frac{L(\text{dry samples}) - L(\text{fired samples})}{L(\text{dry samples})} \times 100 \quad (4)$$

$$MOR (MPa) = \left( \frac{3FL_{ss}}{2bd^3} \right) \quad (5)$$

W is the sample weight (g) and  $\rho$  is the density of water at room temperature (considered as 1 g/cm<sup>3</sup> at 25 °C). L is the sample length (mm). F is the applied force, L<sub>ss</sub> is the length of the support span (mm); b and d are width (mm) and thickness (mm) of the sample, respectively.

Fitted models were evaluated in terms of the relative content of each component in the mixture. Regression models and coefficients were determined at the 5% level of significance. Four simplex-centroid designs (for each physical property) were carried out to evaluate the responses measured from the Archimedes' principle (AP, AD, WA, and  $\Delta L$ ) and the response surface methodology was used for the modeling and analysis of the results.

## Results and discussion

### Compositional and microstructural analysis

The chemical compositions of the raw materials are presented in Table S2. The kaolinitic clay and kaolin waste are essentially composed of silica (SiO<sub>2</sub>), alumina (Al<sub>2</sub>O<sub>3</sub>) and potassium oxide (K<sub>2</sub>O). The high content of SiO<sub>2</sub> and Al<sub>2</sub>O<sub>3</sub> of the kaolinitic clay and kaolin waste highlights the starting materials as potential candidates to be used in the processing of mullite-based ceramics. The purity of the alumina powder derived from calcination of aluminum hydroxide at 1000 °C is found to be around 95%. The alumina is an additional source of ions Al<sup>3+</sup> in the sintering process of mullite ceramics, due to its insufficient amount in the kaolinitic clay and kaolin waste to form stoichiometric mullite (3Al<sub>2</sub>O<sub>3</sub>·2SiO<sub>2</sub>) [13,19,25]. The small increment of K<sub>2</sub>O in the waste in comparison to kaolinitic clay (4.82 wt.% vs. 0.55 wt.%) may explain the relative higher content of mica in the waste material (40.5 wt.% vs. 4.3 wt.%), as previously discussed by Alves et al. [12]. The loss on ignition (LoI) at 1000 °C for the clay (19 wt.%) is significantly higher than for the kaolin waste (5.5 wt.%), which is associated with the burn-out of organic matter and dehydroxylation of kaolinite [26]. Kaolinitic clay and kaolin waste are composed of kaolinite, mica and quartz, as can be seen in detail in our previous work [12].

XRD patterns of samples sintered at 1400 °C are shown in Fig. 2. XRD data of F2, F3 and F6 have been published in a

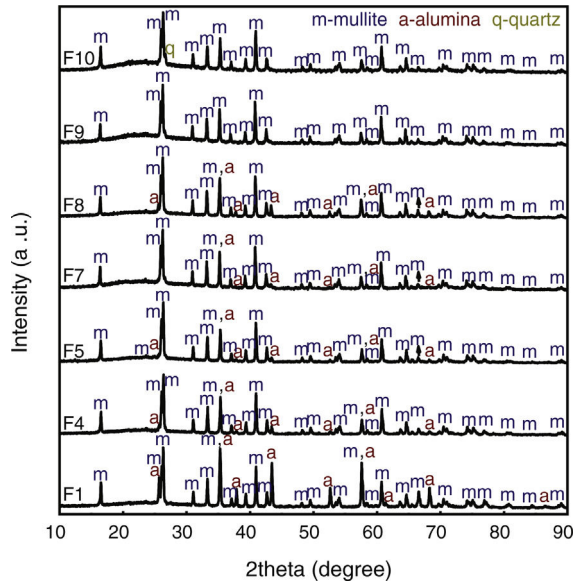


**Fig. 2 – XRD patterns of ceramic formulations sintered at 1400 °C. F1 – 50 wt.% clay and 50 wt.% alumina; F4 – 75 wt.% clay and 25 wt.% alumina; F5 – 50 wt.% clay, 25 wt.% waste and 25 wt.% alumina; F7 – 66.67 wt.% clay, 16.67 wt.% waste and 16.67 wt.% alumina; F8 – 58.33 wt.% clay, 8.33 wt.% waste and 33.33 wt.% alumina; F9 – 83.33 wt.% clay, 8.33 wt.% waste and 8.33 wt.% alumina; F10 – 58.33 wt.% clay, 33.33 wt.% waste and 8.33 wt.% alumina.**

previous article [12] and they are as Supplementary Material (Fig. S1). The crystalline phases identified were mullite (m, reference code 15-0776), quartz (q, reference code 46-1045),

cristobalite (c, reference code 03-0270), and  $\alpha$ -alumina (a, reference code 46-1212). The peaks regarding crystalline phases in formulations 1 and 4 (containing only kaolinitic clay and alumina) were indexed as mullite and alumina. In this situation, the  $\text{SiO}_2$  from kaolinitic clay (crystallized as quartz and cristobalite) react with alumina forming mullite and the excess of  $\text{Al}_2\text{O}_3$  crystallizes as  $\alpha$ -alumina [27,28]. In F2 (kaolinitic clay), the crystalline phases are mullite, quartz and cristobalite. Quartz is transformed into amorphous silica and partially crystallized into cristobalite [29,30]. In alumina-free formulations (2, 3 and 6), the dissolution of silica during sintering saturates the liquid phase, promoting the crystallization of silica polymorphs at the quartz-liquid interface. The two mullite reflections at  $2\theta \approx 26^\circ$  (planes (120) and (210)) are classically attributed to the presence of orthorhombic mullite (secondary mullite) [31]. Formulations 5, 7 and 8 have the same crystalline phases (mullite and alumina). Formulation 9 has only mullite at 1400 °C due to the low amount of alumina (8.33 wt.%). The same behavior was observed in formulation 10, but it also has a residual amount of quartz. The mullitization reaction occurs between the particles of  $\text{Al}_2\text{O}_3$  and  $\text{SiO}_2$  by diffusing  $\text{Al}^{+3}$  and  $\text{Si}^{+4}$  ions through the crystalline lattice [32]. Formulation 10, having more kaolin waste and less alumina than formulation 8, presents the residual quartz phase ( $2\theta \approx 26.7^\circ$ ). In the XRD patterns, the presence of an amorphous silica-rich phase is observed by the amorphous halo in the region of  $2\theta = 15^\circ\text{--}30^\circ$ . Fig. 3 depicts needle-like mullite embedded in the amorphous silica-rich phase for sample F3 (Fig. 3a) and mullite and alumina grains for sample F1 (Fig. 3b). In all formulations with kaolin waste (the vast majority), mullite grains embedded in a glassy phase are expected, as depicts in Fig. 3a. Raw materials with mica in their compositions present an increased amount of liquid phase during the sintering process, which

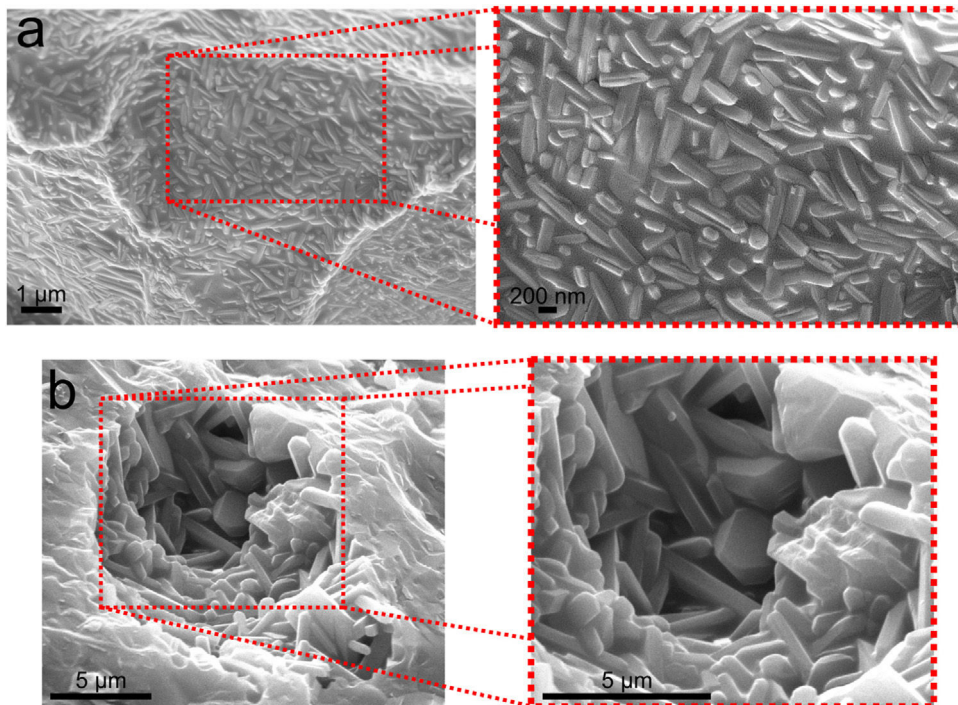


**Fig. 3 – FESEM images of the formulation 3 (50 wt.% clay and 50 wt.% waste) showing needle-like mullite embedded in an amorphous silica-rich phase (a) and the formulation 1 showing mullite and alumina grains (b).**

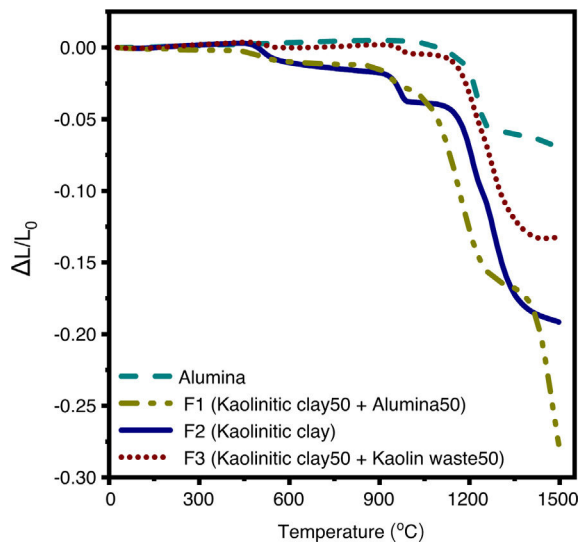


**Fig. 4 – Dilatometric analysis of the samples F1 (50 wt.% clay and 50 wt.% alumina), F2 (100 wt.% clay), F3 (50 wt.% clay and 50 wt.% waste), and alumina. Note: F2 and F3 data were obtained from our previous article [12] for comparison.**

contributes to the dissolution of silica and a glassy phase is then formed [22]. As predicted by the  $\text{SiO}_2\text{-Al}_2\text{O}_3\text{-K}_2\text{O}$  phase diagram,  $\text{K}_2\text{O}$  promotes the occurrence of a peritectic liquid at temperatures higher than  $1140^\circ\text{C}$  [33]. Kim et al. [34] studied the  $\text{K}_2\text{O-Al}_2\text{O}_3\text{-SiO}_2$  system with a thermodynamic optimization of experimental phase diagrams. In their study, the liquid phase was described using the Modified Quasichemical Model with the  $\text{KAlO}_2$  associate component.

### Sintering and technological properties

The sintering shrinkage behavior of the formulation 2 (kaolinitic clay), alumina, formulation 1 (kaolinitic clay and alumina, 1:1), and formulation 3 (kaolinitic clay and kaolin waste, 1:1) was investigated via dilatometric analysis, as seen in Fig. 4. In the formulations 1–3, linear shrinkage of about 1% was observed between  $450$  and  $600^\circ\text{C}$ . This fact is related to the transformation of kaolinite into metakaolinite [35]. F1 and F2 samples are less sensitive to this structural transformation (dehydroxylation of kaolinite) due to the lower kaolinite content when compared to the pure kaolinitic clay [12]. Between  $900$  and  $1000^\circ\text{C}$ , kaolinitic clay shows a shrinkage of around 2%, which corresponds to the nucleation of Al-Si spinel and mullite [36]. In formulations with partial substitution of kaolinitic clay by kaolin waste, this shrinkage is less pronounced. This fact can be explained by an increase in volume during the dehydroxylation of the mica [37]. The dilatometric curve of alumina shows the  $\theta\text{-Al}_2\text{O}_3 \rightarrow \alpha\text{-Al}_2\text{O}_3$  phase transformation at  $1100\text{--}1260^\circ\text{C}$ , in good agreement with the work of Lamouri et al. [38]. As previously reported,  $1500^\circ\text{C}$  is not enough to promote the complete densification of alumina [38]. The sintering process starts at approximately  $1100^\circ\text{C}$  for the clay-based formulations (F1, F2 and F3). The lower shrinkage observed for the F3 compared to the F2 is due to the higher liquid phase content formed in F3 (formulation with kaolin

waste) that accelerates the densification process through a viscous flux mechanism. As previously discussed,  $\text{K}_2\text{O}$  contributes to the formation of a peritectic liquid at temperatures higher than  $1140^\circ\text{C}$ . As is well known, green density of ceramics is about 50–60% [39]. After the firing process, mullite–glass ceramics densify around 90% at  $1400^\circ\text{C}$  [8]. F1 shows events related to the phase transformation of alumina ( $\theta$  to  $\alpha$ ) and the densification process; however, as well as for pure alumina, complete densification was not achieved at  $1500^\circ\text{C}$  due to the amount of alumina in the formulation (50 wt.%).

The physical properties are shown in Table S3. From the analysis of variance (ANOVA, Table 2), the experimental data were well fitted to the full cubic model.

Statistical significance can be investigated through the analysis of the relevant statistical parameters ( $R^2$ , P-value, and F-test). The ratio of the regression sum of squares and the total sum of squares,  $R^2$ , is attributed to the correlation between the observed response and the value predicted by the adjusted model. For the fitted models, the  $R^2$  values of linear firing shrinkage, water absorption, apparent porosity and apparent density were 97.78%, 97.77%, 98.42%, and 94.29%, respectively; however,  $R^2$  must not be compared with 100% and pure error must be discounted [40]. Therefore, those  $R^2$  values must be compared with 97.83%, 98.21%, 98.77%, and 98.13%, respectively (these values were obtained as follows:  $(\text{Sum of squares}_{\text{total}} - \text{Sum of squares}_{\text{pure error}}) / \text{Sum of squares}_{\text{total}}$ ). These percentages are close to 100% because the contribution of pure error is relatively small. The ratios between the model mean square and the residual mean square for the linear firing shrinkage, water absorption, apparent porosity and apparent density were 170.99, 200.33, 241.72, and 75.45, respectively. Therefore, for linear firing shrinkage ( $F_{8,31} = 2.26$ ), water absorption ( $F_{7,32} = 2.31$ ), apparent porosity ( $F_{8,31} = 2.26$ ), and apparent density ( $F_{7,32} = 2.31$ ), the regressions are highly significant, at the 5% level of significance [40]. However, for the apparent density, the ratio between the lack of fit mean square and the pure error mean square (30.93) compared to the F distribution ( $F_{2,30} = 3.32$ ) showed that the model exhibits a considerable lack of fit and, in this case, the model is not effective in making reliable predictions.

Through the results, regression equations (in terms of pseudo components) for the physical properties were obtained. These Eqs. (6)–(8) are valid for the ranges of each raw material studied here (Table S1). In these equations, A, C, and W correspond to the pseudo component values (0–1): alumina, kaolinitic clay and kaolin waste, respectively.

$$\Delta L(\%) = 15.47A + 10.95C + 9.28W + 5.65AC + 6.41AW + 9.09CW + 28.81ACW - 28.14AC(A - C) - 8.10AW(A - W) \quad (6)$$

$$WA(\%) = 13.57A + 3.59C + 0.47W - 8.88AC - 28.87AW - 5.15CW + 35.26AC(A - C) - 16.68AW(A - W) \quad (7)$$

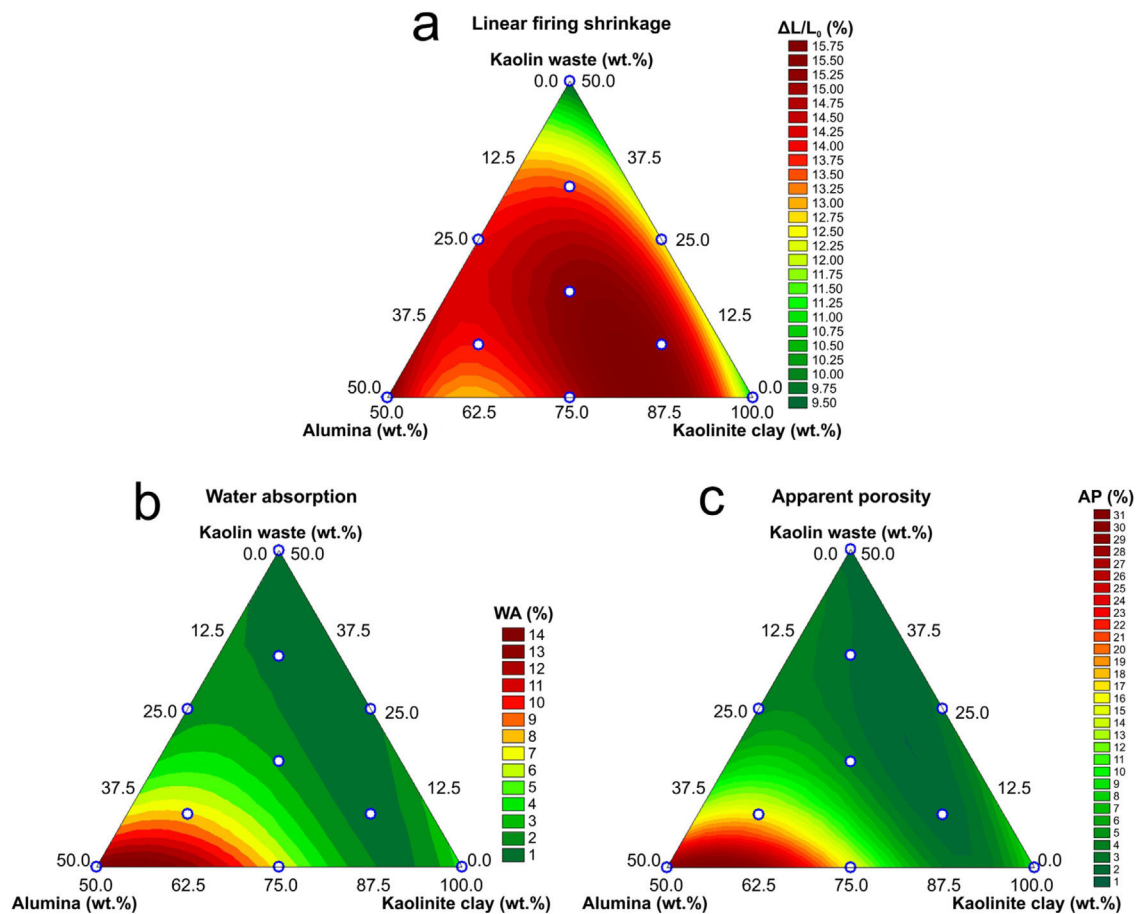
$$AP(\%) = 29.07A + 8.58C + 1.05W - 14.31AC - 45.89AW - 9.24CW - 44.08ACW + 85.12AC(A - C) - 42.36AW(A - W) \quad (8)$$

**Table 2 – ANOVA for the fit of the data in Table S3.**

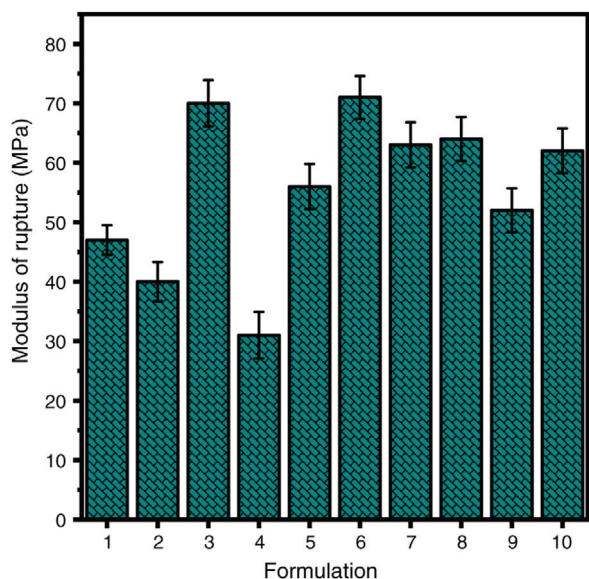
Response	Source	Sum of squares	Degree of freedom	Mean square	F value
$\Delta L$	Model	150.5985	8	18.8248	170.9915
	Residual	3.4129	31	0.1101	–
	Lack of fit	0.0736	1	0.0736	0.6613
	Pure error	3.3393	30	0.1113	–
	Total	154.0114	39	3.9490	–
WA	Model	651.8333	7	93.1190	200.3337
	Residual	14.8742	32	0.4648	–
	Lack of fit	2.9734	2	1.4867	3.7478
	Pure error	11.9008	30	0.3967	–
	Total	666.7075	39	17.0951	–
AP	Model	3011.0613	8	376.3827	241.7216
	Residual	48.2698	31	1.5571	–
	Lack of fit	10.6655	1	10.6655	8.5087
	Pure error	37.6044	30	1.2535	–
	Total	3059.3311	39	78.4444	–
AD	Model	0.7921	7	0.1132	75.4504
	Residual	0.0480	32	0.0015	–
	Lack of fit	0.0323	2	0.0162	30.9258
	Pure error	0.0157	30	0.0005	–
	Total	0.8401	39	0.0215	–

Fig. 5 shows the response surfaces described by Eqs. (6)–(8). In Fig. 5(a), it was possible to observe that formulations with higher kaolin waste content have lower firing shrinkage. This fact can be explained by the liquid phase-assisted sintering

mechanism activated by the increased amount of mica from the kaolin waste and therefore filling the open pores [8,13]. From Fig. 5(b, c), a lower open porosity (thereby, water absorption) is observed in formulations with higher kaolin waste content due to the liquid phase-assisted sintering mechanism.



**Fig. 5 – Response surfaces for the (a) linear firing shrinkage, (b) water absorption, and (c) apparent porosity.**



**Fig. 6 – Modulus of rupture of the ceramic formulations sintered at 1400 °C. F1 – 50 wt.% clay and 50 wt.% alumina; F2 – 100 wt.% clay; F3 – 50 wt.% clay and 50 wt.% waste; F4 – 75 wt.% clay and 25 wt.% alumina; F5 – 50 wt.% clay, 25 wt.% waste and 25 wt.% alumina; F6 – 75 wt.% clay and 25 wt.% waste; F7 – 66.67 wt.% clay, 16.67 wt.% waste and 16.67 wt.% alumina; F8 – 58.33 wt.% clay, 8.33 wt.% waste and 33.33 wt.% alumina; F9 – 83.33 wt.% clay, 8.33 wt.% waste and 8.33 wt.% alumina; F10 – 58.33 wt.% clay, 33.33 wt.% waste and 8.33 wt.% alumina. Note: Data of F2, F3 and F6 were obtained from our previous work [12] for comparison.**

On the other hand, solid phase-assisted sintering mechanism is observed for formulations with high alumina content (mullite–alumina composites, Fig. 3b), as reported in a previous work [13]. Formulations with a higher waste content show lower shrinkage and lower porosity due to the liquid that fills the pores, reaching complete densification faster than formulations with a higher alumina content (lower waste content).

Our group has recently studied the electrical–dielectric properties of mullite–glass composites from mixtures of a kaolinitic clay and kaolin waste [8,41]. Ribeiro et al. [42] also studied the electrical properties of mullite–alumina ceramics with the presence of a glassy phase. In all these studies, interesting microstructure–electrical relationships as a function of glass content have been highlighted in mullite-based ceramics. Therefore, from the statistical analysis, it is possible to determine the appropriate formulations according to the target application, e.g., electronics-related applications.

The modulus of rupture of the ceramic formulations is shown in Fig. 6. The lowest values are obtained in kaolin waste-free formulations (F1, F2 and F4). In formulations with kaolin waste, liquid phase sintering is activated and the liquid fills the open pores (as shown in Fig. 5(c)), which leads to an increase in modulus.

## Conclusions

The simplex-centroid mixture design was successfully used to prepare mullite–glass ceramics after sintering at 1400 °C. The microstructural analysis revealed mullite, residual quartz, cristobalite, and  $\alpha$ -alumina as the main crystalline phases of the samples derived from kaolin, kaolin waste, and alumina. An amorphous silica-rich phase was observed after sintering of raw materials with the presence of mica in their compositions. Statistical analysis proved to be adequate to obtain statistical models, highly significant, which correlate the concentrations of raw materials with linear firing shrinkage, water absorption, and apparent porosity. In kaolin waste-rich formulations, a liquid phase assisted sintering mechanism favors the densification process, improving the mechanical strength of the ceramics. While high concentrations of alumina increase the water absorption and apparent porosity of the samples.

## Funding

This study was financed in part by the Coordenação de Aperfeiçoamento de Pessoal de Nível Superior - Brasil (CAPES) - Finance Code 001.

## Appendix A. Supplementary data

Supplementary data associated with this article can be found, in the online version, at [doi:10.1016/j.bsecv.2020.09.002](https://doi.org/10.1016/j.bsecv.2020.09.002)

## REFERENCES

- [1] H. Schneider, J. Schreuer, B. Hildmann, Structure and properties of mullite—a review, *J. Eur. Ceram. Soc.* 28 (2008) 329–344, [http://dx.doi.org/10.1016/j.jeurceramsoc.2007.03.017](https://doi.org/10.1016/j.jeurceramsoc.2007.03.017).
- [2] T.F. Choo, M.A.M. Salleh, K.Y. Kok, K.A. Matori, A review on synthesis of mullite ceramics from industrial wastes, *Recycling 4* (2019) 39, [http://dx.doi.org/10.3390/recycling4030039](https://doi.org/10.3390/recycling4030039).
- [3] P. Bueno, K. Pagnan Furlan, D. Hotza, R. Janssen, High-temperature stable inverse opal photonic crystals via mullite–sol-gel infiltration of direct photonic crystals, *J. Am. Ceram. Soc.* 102 (2019) 686–694, [http://dx.doi.org/10.1111/jace.16012](https://doi.org/10.1111/jace.16012).
- [4] Y. Li, J. Lu, Y. Zeng, Z. Liu, C. Wang, Preparation and characterization of mullite powders from coal fly ash by the mullitization and hydrothermal processes, *Mater. Chem. Phys.* 213 (2018) 518–524, [http://dx.doi.org/10.1016/j.matchemphys.2018.04.056](https://doi.org/10.1016/j.matchemphys.2018.04.056).
- [5] F.J. Pérez, M.P. Hierro, M.C. Carpintero, F.J. Bolívar, Aluminum and silicon co-deposition by the chemical vapor deposition in fluidized bed reactor technique as a precursor of protective coatings of mullite, *Surf. Coat. Technol.* 184 (2004) 361–369, [http://dx.doi.org/10.1016/j.surfcoat.2003.11.001](https://doi.org/10.1016/j.surfcoat.2003.11.001).
- [6] M.F. Serra, M.S. Conconi, M.R. Gauna, G. Suárez, E.F. Aglietti, N.M. Rendtorff, Mullite ( $3Al_2O_3 \cdot 2SiO_2$ ) ceramics obtained by reaction sintering of rice husk ash and alumina, phase evolution, sintering and microstructure, *J. Asian Ceram. Soc.*

- 4 (1) (2016) 61–67, <http://dx.doi.org/10.1016/j.jascer.2015.11.003>.
- [7] E.P. de Almeida, I.P. de Brito, H.C. Ferreira, H.L. Lira, L.N. de Lima Santana, G. de Araújo Neves, Cordierite obtained from compositions containing kaolin waste, talc and magnesium oxide, *Ceram. Int.* 44 (2018) 1719–1725, <http://dx.doi.org/10.1016/j.ceramint.2017.10.102>.
- [8] R.M. Andrade, A.J.M. Araújo, H.P.A. Alves, J.P.F. Grilo, R.P.S. Dutra, L.F.A. Campos, D.A. Macedo, On the physico-mechanical, electrical and dielectric properties of mullite–glass composites, *Ceram. Int.* 45 (2019) 18509–18517, <http://dx.doi.org/10.1016/j.ceramint.2019.06.070>.
- [9] R.R. Menezes, H.G.M. Neto, L.N.L. Santana, H.L. Lira, H.S. Ferreira, G.A. Neves, Optimization of wastes content in ceramic tiles using statistical design of mixture experiments, *J. Eur. Ceram. Soc.* 28 (2008) 3027–3039, <http://dx.doi.org/10.1016/j.jeurceramsoc.2008.05.007>.
- [10] A.Á.B. Maia, R.N. Dias, R.S. Angélica, R.F. Neves, Influence of an aging step on the synthesis of zeolite NaA from Brazilian Amazon kaolin waste, *J. Mater. Res. Technol.* 8 (2019) 2924–2929, <http://dx.doi.org/10.1016/j.jmrt.2019.02.021>.
- [11] P.R.S. de Castro, A.Á.B. Maia, R.S. Angélica, Study of the thermal stability of faujasite zeolite synthesized from kaolin waste from the Amazon, *Mater. Res.* 22 (2019) 321, <http://dx.doi.org/10.1590/1980-5373-mr-2019-0321>.
- [12] H.P.A. Alves, J.B. Silva, L.F.A. Campos, S.M. Torres, R.P.S. Dutra, D.A. Macedo, Preparation of mullite based ceramics from clay–kaolin waste mixtures, *Ceram. Int.* 42 (2016) 19086–19090, <http://dx.doi.org/10.1016/j.ceramint.2016.09.068>.
- [13] A.J.M. Araújo, H.P.A. Alves, R.M. Andrade, L.F.A. Campos, D.A. Macedo, A.L.S. Pinho, R.M. Nascimento, C.A. Paskocimas, Designing experiments for the optimization of solid-state synthesis and characterization of alumina-based composites, *Ceram. Int.* 45 (2019) 8525–8532, <http://dx.doi.org/10.1016/j.ceramint.2019.01.166>.
- [14] M. Arzani, H.R. Mahdavi, O. Bakhtiari, T. Mohammadi, Preparation of mullite ceramic microfilter membranes using response surface methodology based on central composite design, *Ceram. Int.* 42 (2016) 8155–8164, <http://dx.doi.org/10.1016/j.ceramint.2016.02.022>.
- [15] A.D. Noni Jr., D. Hotza, V.C. Soler, E.S. Vilches, Influence of composition on mechanical behaviour of porcelain tile. Part I: Microstructural characterization and developed phases after firing, *Mater. Sci. Eng. A* 527 (2010) 1730–1735, <http://dx.doi.org/10.1016/j.msea.2009.10.057>.
- [16] R.G. Frizzo, A. Zaccaron, V. de Souza Nandi, A.M. Bernardin, Pyroplasticity on porcelain tiles of the albite-potassium feldspar–kaolin system: a mixture design analysis, *J. Build. Eng.* 31 (2020) 101432, <http://dx.doi.org/10.1016/j.jobbe.2020.101432>.
- [17] D.C. Montgomery, *Design and Analysis of Experiments*, 8th ed., John Wiley & Sons, Inc., 2013.
- [18] R.B. Bagwell, G.L. Messing, Critical factors in the production of sol–gel derived porous alumina, *Key Eng. Mater.* 115 (1995) 45–64, <http://dx.doi.org/10.4028/www.scientific.net/KEM.115.45>.
- [19] Z.-Y. Deng, T. Fukasawa, M. Ando, G.-J. Zhang, T. Ohji, High-surface-area alumina ceramics fabricated by the decomposition of Al(OH)<sub>3</sub>, *J. Am. Ceram. Soc.* 84 (2001) 485–491, <http://dx.doi.org/10.1111/j.1151-2916.2001.tb00687.x>.
- [20] A. Yamuna, S. Devanarayanan, M. Lalithambika, Phase-pure mullite from kaolinite, *J. Am. Ceram. Soc.* 85 (2002) 1409–1413, <http://dx.doi.org/10.1111/j.1151-2916.2002.tb00289.x>.
- [21] C.Y. Chen, G.S. Lan, W.H. Tuan, Preparation of mullite by the reaction sintering of kaolinite and alumina, *J. Eur. Ceram. Soc.* 20 (2000) 2519–2525, [http://dx.doi.org/10.1016/S0955-2219\(00\)00125-4](http://dx.doi.org/10.1016/S0955-2219(00)00125-4).
- [22] H.P.A. Alves, R.A. Junior, L.F.A. Campos, R.P.S. Dutra, J.P.F. Grilo, F.J.A. Loureiro, D.A. Macedo, Structural study of mullite based ceramics derived from a mica-rich kaolin waste, *Ceram. Int.* 43 (2017) 3919–3922, <http://dx.doi.org/10.1016/j.ceramint.2016.12.035>.
- [23] ASTM C674-13(2018), Standard Test Methods for Flexural Properties of Ceramic Whiteware Materials, ASTM International, West Conshohocken, PA, 2018, <http://dx.doi.org/10.1520/C0674-13R18>.
- [24] P.S. Santos, *Ciência e tecnologia de argilas*, 2nd ed., Edgard Blucher Ltda, São Paulo, 1989.
- [25] S.G. Medeiros, R.P.S. Dutra, J.P.F. Grilo, A.E. Martinelli, C.A. Paskocimas, D.A. Macedo, Preparation of low-cost alumina–mullite composites via reactive sintering between a kaolinite clay from Paraíba and aluminum hydroxide, *Cerâmica* 62 (2016) 266–271, <http://dx.doi.org/10.1590/0366-69132016623631992>.
- [26] E. Gasparini, S.C. Tarantino, P. Ghigna, M.P. Riccardi, E.I. Cedillo-González, C. Siligardi, M. Zema, Thermal dehydroxylation of kaolinite under isothermal conditions, *Appl. Clay Sci.* 80–81 (2013) 417–425, <http://dx.doi.org/10.1016/j.clay.2013.07.017>.
- [27] Z. Hou, B. Cui, L. Liu, Q. Liu, Effect of the different additives on the fabrication of porous kaolin-based mullite ceramics, *Ceram. Int.* 42 (2016) 17254–17258, <http://dx.doi.org/10.1016/j.ceramint.2016.08.020>.
- [28] J. Bai, Fabrication and properties of porous mullite ceramics from calcined carbonaceous kaolin and  $\alpha$ -Al<sub>2</sub>O<sub>3</sub>, *Ceram. Int.* 36 (2010) 673–678, <http://dx.doi.org/10.1016/j.ceramint.2009.10.006>.
- [29] V.A. Alexeyev, L.S. Medvedeva, N.P. Starshinova, Paradoxical transformation of the equilibrium quartz–water system into an unequilibrated one, *Geochem. Int.* 51 (2013) 382–404, <http://dx.doi.org/10.1134/S0016702913050029>.
- [30] G.D. Nipan, Phase states of Li/W/Mn/SiO<sub>2</sub> composites in catalytic oxidative coupling of methane, *Inorg. Mater.* 51 (2015) 389–395, <http://dx.doi.org/10.1134/S002016851504010X>.
- [31] M.A. Sainz, F.J. Serrano, J.M. Amigo, J. Bastida, A. Caballero, XRD microstructural analysis of mullites obtained from kaolinite–alumina mixtures, *J. Eur. Ceram. Soc.* 20 (2000) 403–412, [http://dx.doi.org/10.1016/S0955-2219\(99\)00183-1](http://dx.doi.org/10.1016/S0955-2219(99)00183-1).
- [32] G.C. Ribeiro, B.A. Fortes, L. da Silva, J.A. Castro, S. Ribeiro, Evaluation of mechanical properties of porous alumina ceramics obtained using rice husk as a porogenic agent, *Cerâmica* 65 (2019) 70–74, <http://dx.doi.org/10.1590/0366-6913201965s12604>.
- [33] G.L. Lecomte-Nana, J.P. Bonnet, P. Blanchart, Investigation of the sintering mechanisms of kaolin–muscovite, *Appl. Clay Sci.* 51 (2011) 445–451, <http://dx.doi.org/10.1016/j.clay.2011.01.007>.
- [34] D.-G. Kim, B. Konar, I.-H. Jung, Thermodynamic optimization of the K<sub>2</sub>O–Al<sub>2</sub>O<sub>3</sub>–SiO<sub>2</sub> system, *Ceram. Int.* 44 (2018) 16712–16724, <http://dx.doi.org/10.1016/j.ceramint.2018.06.099>.
- [35] H. Peng, J. Vaughan, J. Vogrin, The effect of thermal activation of kaolinite on its dissolution and re-precipitation as zeolites in alkaline aluminate solution, *Appl. Clay Sci.* 157 (2018) 189–197, <http://dx.doi.org/10.1016/j.clay.2018.03.002>.
- [36] Y.F. Chen, M.C. Wang, M.H. Hon, Phase transformation and growth of mullite in kaolin ceramics, *J. Eur. Ceram. Soc.* 24 (2004) 2389–2397, [http://dx.doi.org/10.1016/S0955-2219\(03\)00631-9](http://dx.doi.org/10.1016/S0955-2219(03)00631-9).
- [37] S. Udagawa, K. Urabe, H. Hasu, The crystal structure of muscovite dehydroxylate, *J. Jpn. Assoc. Mineral. Petrol. Econ. Geol.* 69 (1974) 381–389, <http://dx.doi.org/10.2465/ganko1941.69.381>.

- [38] S. Lamouri, M. Hamidouche, N. Bouaouadja, H. Belhouchet, V. Garnier, G. Fantozzi, J.F. Trelkat, Control of the  $\gamma$ -alumina to  $\alpha$ -alumina phase transformation for an optimized alumina densification, *Bol. La Soc. Española Ceram. Vidr.* 56 (2017) 47–54, <http://dx.doi.org/10.1016/j.bsecv.2016.10.001>.
- [39] L.F. Francis, Powder processes, in: *Mater. Process. A Unified Approach to Process*, *Met. Ceram. Polym.*, 2016, pp. 343–414, <http://dx.doi.org/10.1016/b978-0-12-385132-1.00005-7> (Chapter 5).
- [40] B.B. Neto, I.S. Scarminio, R.E. Bruns, Empirical model-building, in: *Data Handl. Sci. Technol.*, Elsevier, 2005, pp. 199–244, [http://dx.doi.org/10.1016/S0922-3487\(05\)25005-0](http://dx.doi.org/10.1016/S0922-3487(05)25005-0) (Chapter 5).
- [41] J.P.F. Grilo, H.P.A. Alves, A.J.M. Araújo, R.M. Andrade, R.P.S. Dutra, D.A. Macedo, Dielectric and electrical properties of a mullite/glass composite from a kaolinite clay/mica-rich kaolin waste mixture, *Cerâmica* 65 (2019) 117–121, <http://dx.doi.org/10.1590/0366-69132019653732648>.
- [42] M.J. Ribeiro, J.C.C. Abrantes, J.M. Ferreira, J.A. Labrincha, Predicting processing-sintering-related properties of mullite–alumina ceramic bodies based on Al-rich anodising sludge by impedance spectroscopy, *J. Eur. Ceram. Soc.* 24 (2004) 3841–3848, <http://dx.doi.org/10.1016/j.jeurceramsoc.2003.12.026>.